

Semi-hadronic Tau Decays at CLEO

Alan. J. Weinstein ^{a *}

^aCalifornia Institute of Technology,
Pasadena, CA 91125, USA
Representing the CLEO Collaboration

We describe recent results from the CLEO experiment on semi-hadronic decays of the tau lepton. We discuss the analysis of sub-structure in the decays $\tau^- \rightarrow \pi^- \pi^0 \nu_\tau$, $(3\pi)^- \nu_\tau$, $(4\pi)^- \nu_\tau$, $(6\pi)^- \nu_\tau$, and $\eta X^- \nu_\tau$. Various applications of these results are also discussed.

This contribution reviews several new or updated results on substructure in semi-hadronic tau decays, recently published by the CLEO Collaboration. These results are all based on data collected with the CLEO detector at Cornell's CESR collider, in the reaction $e^+e^- \rightarrow \tau^+\tau^-$ at $\sqrt{s} \simeq 10.6$ GeV. Most of these results are based on $\approx 4.3 \times 10^6$ $\tau^+\tau^-$ pairs collected with the CLEO II detector between 1990 — 1995. Some (where noted) also use $\approx 8.0 \times 10^6$ $\tau^+\tau^-$ pairs collected with the CLEO II.V detector (which includes a silicon vertex detector and better drift chamber tracking) between 1995 — 1999.

1. Hadronic substructure of tau decays

All the tau decay branching fractions larger than 1% have been measured reasonably well, with errors that are dominated by systematic uncertainties. The next step in exploiting tau decays to learn more about the Standard Model is to explore the substructure of the decays to three or more final state particles.

For the leptonic decays $\tau \rightarrow \ell \bar{\nu}_\ell \nu_\tau$, the substructure is parameterized by the Michel parameters; precision measurements of these serve to constrain the charged weak couplings of the tau, beyond the well-understood Standard Model $V - A$ couplings.

For the semi-hadronic decays $\tau \rightarrow X \nu_\tau$, the study of hadronic substructure is a clean probe

*Work supported by the US Department of Energy and National Science Foundation.

of one of the least well understood aspects of the Standard Model: low energy meson dynamics.

In tau semi-hadronic decays, momentum transfers are small, so final states are dominated by resonances (vector, axial-vector, and to a lesser extent, scalar and tensor resonances); see Fig. 1. Lacking a fundamental theory of meson resonance dynamics, these processes are described using models.

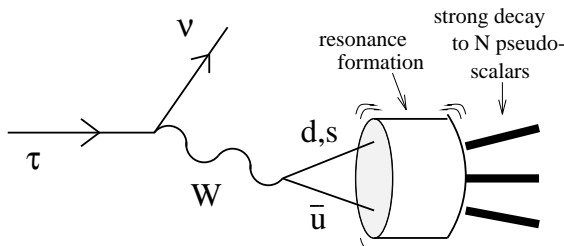


Figure 1. Cartoon of semi-hadronic tau decay to mesonic final states dominated by intermediate resonances.

The weak decay $\tau^- \rightarrow W^{*-} \nu_\tau$ (and its charged conjugate, which is implicitly assumed throughout this paper) is assumed to be well described by the Standard Model $V - A$ current, and the

poorly-known hadronic physics in the transition $W^{*-} \rightarrow X^-$, where X is a system of hadrons, is described by a spectral function $v(q^2)$ [1,2], where $q^2 \equiv M_X^2$ is the invariant mass squared of the hadronic system. The ‘‘production’’ and ‘‘decay’’ of the X^- system separates cleanly; for decay to non-strange final states,

$$\frac{d\Gamma}{dq^2} = \frac{G_F^2 |V_{ud}|^2}{32\pi^2 M_\tau^3} (M_\tau^2 - q^2)^2 (M_\tau^2 + 2q^2) v(q^2), (1)$$

with an analogous expression for Cabibbo-suppressed decays. The spectral function contains all the strong interaction dynamics.

CLEO can measure $v(q^2)$ using exclusive final states like $X = 2\pi, 3\pi, \text{etc.}$; it is more problematic to do inclusive studies, due to backgrounds and cross-feeds between different exclusive final states.

1.1. Theory of tau semi-hadronic decays

The low-energy dynamics of strongly-interacting mesons is the poorest understood aspect of the Standard model. The tools that we have to understand the structure of the spectral function $v(q^2)$ are: Conservation laws (Lorentz invariance, isospin, $SU(3)_f$, G -parity, *etc.*); resonance dominance models and the PDG catalog; the Conserved Vector Current (CVC) constraints; QCD sum rules (for inclusive studies); Chiral perturbation theory of pseudoscalar mesons and higher mass resonances (applicable only for momenta close to threshold); QCD on the lattice; and non-perturbative models inspired by S-matrix theory.

For $\tau^- \rightarrow \nu_\tau \bar{u}d$ (*i.e.*, with strangeness = 0), the strong hadronization of the $\bar{u}d$ into observable mesons conserves parity, isospin, and G -parity, so that J^P, I^G are good quantum numbers of the hadronic current from weak decays [1,2]. The weak vector current produces systems of pions with $J^P = 0^+$ or 1^- , even G parity, and even numbers of pions. The weak axial-vector current produces systems of pions with $J^P = 0^-$ or 1^+ , odd G parity, and odd numbers of pions.

CVC relates the vector part of $W^{*-} \rightarrow \bar{u}d$ in, *e.g.*, $\tau^- \rightarrow X_{had}^- \nu_\tau$ to the isovector $I = 1$ part of

$\gamma^* \rightarrow \bar{u}u, \bar{d}d$ in *e.g.*, $e^+e^- \rightarrow X_{had}^0$, with $s = q^2$:

$$\sigma_{e^+e^- \rightarrow X^0}^{(I=1)}(s) = \left(\frac{4\pi^2 \alpha^2}{s} \right) v_X(s). (2)$$

CVC also forbids $J^P = 0^+$ final states from forming. The axial-vector current is not so heavily constrained (PCAC, sum rules); tau lepton decay is well suited for study of light axial vector mesons.

2. $\tau^- \rightarrow \pi^- \pi^0 \nu_\tau$

We expect the 2π final state to be dominated by the vector resonances $\rho(770)$, and its (broad and thus poorly understood) radial excitations $\rho'(1450), \rho''(1700)$. The masses, pole widths, and mass-dependent widths of these resonances are of interest. It is also of interest to search for unexpected (CVC-violating) scalar resonances, or non-resonant contributions with well-defined Lorentz structure.

The recently published results from CLEO [3] are based on the CLEO-II sample of 4.3×10^6 produced tau pairs. Approximately 87,000 events consistent with $\tau^\mp \rightarrow \pi^\mp \pi^0 \nu_\tau$ were selected. The $\pi\pi^0$ mass distribution is shown in Fig. 2.

This mass distribution (with $q^2 = m^2(\pi\pi)$) is modeled in terms of the spectral function:

$$v_{\pi\pi}(q^2) = \frac{1}{12\pi} |F_\pi(q^2)|^2 \left(\frac{2p_\pi}{\sqrt{q^2}} \right)^3, (3)$$

where $F_\pi(q^2)$ is the pion charged-current form-factor. CVC predicts that this form factor should be the same (up to isospin-violating effects) as the neutral current form factor for $\gamma \rightarrow \pi^+\pi^-$, whose value at $q^2 = 0$ is equal to 1. We have allowed $F_\pi(0)$ to float in our fits, although it has been argued [4] that a better approach is to fix it to its predicted value and extrapolate to $q^2 > 4m_\pi^2$ in some smooth and well defined way.

2.1. Model-dependent fits

CLEO has used two phenomenological models of $F_\pi(q^2)$ to fit the observed spectrum. In the model of Kühn and Santamaria (K&S, [5]), $F_\pi(q^2)$ is a coherent sum of simple Breit-Wigner lineshapes:

$$F_\pi(q^2) \propto BW_\rho + \beta BW_{\rho'} + \gamma BW_{\rho''} + \dots, (4)$$

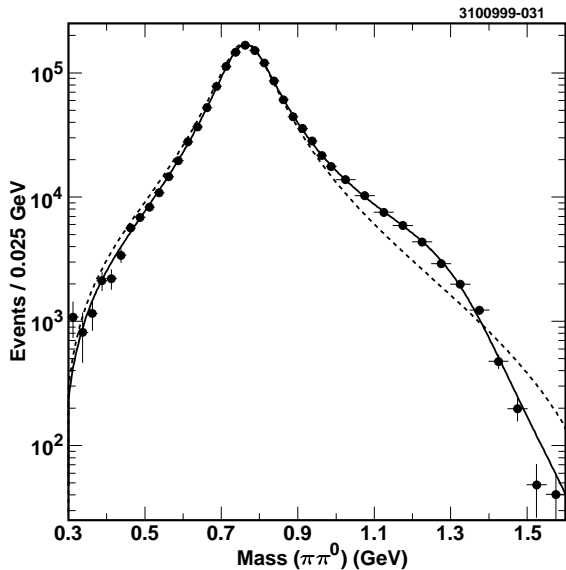


Figure 2. The $\pi\pi^0$ mass distribution, based on 87,000 events observed by CLEO. The points are data, corrected for efficiency, background, and resolution (via an unfold procedure). The solid curve is a fit (described in the text) including contributions from the $\rho(770)$, $\rho(1450)$, $\rho(1700)$ resonances. The dashed curve is a fit with the $\rho(770)$ lineshape only.

$$BW_\rho = \frac{M_\rho^2}{(M_\rho^2 - q^2) - i\sqrt{q^2}\Gamma_\rho(q^2)}. \quad (5)$$

The q^2 -dependence of the width $\Gamma_\rho(q^2)$ is calculated assuming simple P-wave decay into two pions, only.

The model of Gounaris and Sakurai (G&S, [6]) is somewhat more complicated, based on assumed effective range formula for the P-wave $\pi\pi$ scattering phase shift.

In both models, the masses and pole widths of the resonances are free (fit) parameters. Since there is negligible sensitivity to the pole mass and width of the ρ'' , they are fixed to be 1700 MeV and 235 MeV, respectively.

The CLEO results favor the G&S model over K&S model. The results of the fits are given in

Table 1

Results of the fits to the CLEO $\tau \rightarrow \pi\pi\nu_\tau$ data using the G&S (ref. [6]) model. The results are compared with analogous results from ALEPH (ref. [7]) and from e^+e^- data (ref. [5]).

	G&S Model		
	CLEO	ALEPH	e^+e^-
M_ρ	775.1 (1.1)	776.4 (0.9)	776
Γ_ρ	150.4 (1.4)	150.5 (1.6)	151
β	-0.121 (10)	-0.077 (8)	-0.052
$M_{\rho'}$	1406 (15)	1400 (16)	1330
$\Gamma_{\rho'}$	455 (41)	$\equiv 310$	270
γ	0.032 (9)	0.001 (9)	-0.031
$ F_\pi(0) ^2$	1.03 (2)	$\equiv 1$	$\equiv 1$
χ^2/dof	22.9/23	54/65	151/132

Table 1, in the context of that model, and are compared with analogous results from ALEPH (using $\tau \rightarrow \pi\pi\nu_\tau$) [7] and a fit to $e^+e^- \rightarrow \pi^+\pi^-$ data in Ref. [5].

These fits yield rather precise values for the charged $\rho(770)$ mass and width (the e^+e^- results are for the ρ^0). The mass of the $\rho(1450)$ is around ~ 1400 MeV, but this is a very model-dependent result, strongly influenced by the presence or absence of the $\rho(1700)$.

2.2. Test of CVC with $|F_\pi(q^2)|^2$

The results of the fit to the CLEO data can be compared directly with the e^+e^- data, as a test of CVC. These comparisons are shown in Figs. 3 and 4. In these figures, $|F_\pi(q^2)|^2$ is extracted directly from CLEO τ data. The $I = 0$ contribution from $\omega \rightarrow \pi^+\pi^-$, including $\rho - \omega$ interference, is removed from e^+e^- data.

We see that the τ data follow the e^+e^- data shape very well, but the e^+e^- data lie $\sim 3\%$ below τ data, throughout the spectrum. This is also seen in the fit of CLEO tau data to the G&S model, where $|F_\pi(0)|^2 \simeq 1.03$, and is consistent with the discrepancy between the world average [8] branching fraction $\mathcal{B}(\tau \rightarrow \pi\pi\nu_\tau)$ and the prediction from CVC with the e^+e^- data [9]:

$$\mathcal{B}(\tau \rightarrow \pi\pi^0\nu) = (25.32 \pm 0.15)\% \quad (6)$$

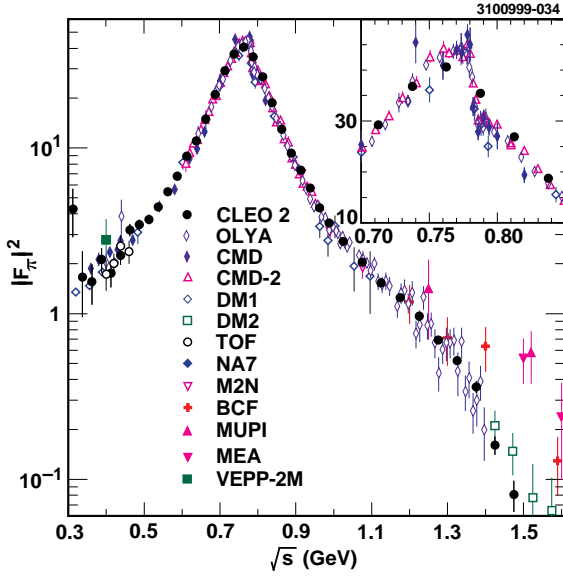


Figure 3. Comparison of $|F_\pi(q^2)|^2$ as determined from CLEO τ data (filled circles), with that obtained from $e^+e^- \rightarrow \pi^+\pi^-$ cross-sections measured at VEPP and Adone.

$$\text{CVC} : \quad (24.52 \pm 0.33)\% \quad (7)$$

$$\Delta \sim 3.2 \pm 1.5\%. \quad (8)$$

If one assumes CVC, the data from tau decays on $|F_\pi(q^2)|^2$ can be used to improve the prediction for the contribution of hadronic vacuum polarization to the anomalous magnetic moment of the muon, $g_\mu - 2$ [10]. Such an improvement is much needed in order to make use of the precision of the BNL E821 ($g_\mu - 2$) experiment to test for electroweak and beyond SM contributions. The CLEO results can be used to improve this prediction, but it has been suggested that allowing $|F_\pi(0)|$ to float is not the appropriate way to make use of the data [4].

3. $\tau \rightarrow 3\pi\nu_\tau$

From conservation of G-parity and parity, we expect the resonance X in $\tau \rightarrow X\nu \rightarrow 3\pi\nu$ to have $J^P = 0^-$ or 1^+ . The vector ($J^P = 1^-$

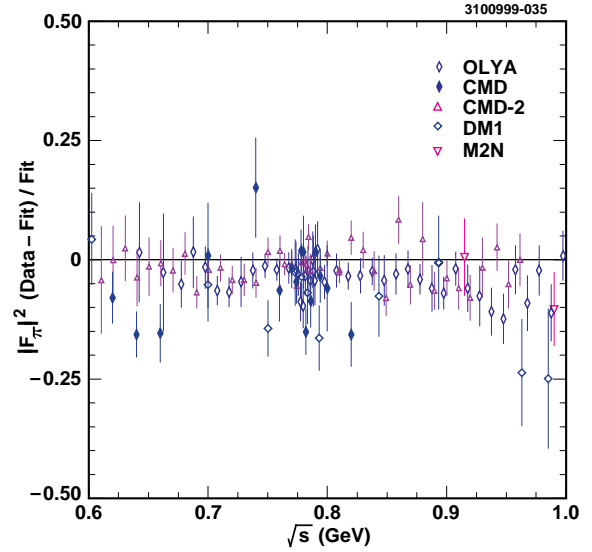


Figure 4. Difference between $|F_\pi(q^2)|^2$ as determined from CLEO τ data, with that obtained from $e^+e^- \rightarrow \pi^+\pi^-$ cross-section measurements.

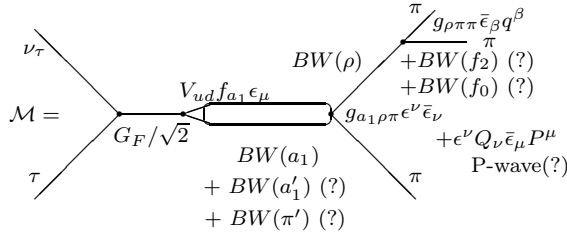
current to $(3\pi)^-$ is forbidden by Bose symmetry (there are two identical pions in the final state). The axial-vector 1^+ current is expected to be dominated by the (broad and thus poorly understood) $a_1(1260)$ meson ($\Gamma_{a_1} \sim 400$ MeV). There may also be a pseudoscalar (0^-) current, *e.g.*, $\pi'^- \rightarrow (3\pi)^-$; but such a current is not conserved ($P_\mu J_{0-}^\mu \neq 0$), so the 0^- current is suppressed by PCAC.

In the simplest models, *e.g.* the Kühn & Santamaria model [5], the a_1 decays to $\rho\pi$ via S-wave. From this, one predicts approximately equal rates to $\pi^-\pi^+\pi^-$ and $\pi^-\pi^0\pi^0$. Kühn and Wagner [11] pointed out that the interference between amplitudes with identical pions permits the measurement of the *sign* of the a_1 helicity, and thus can be used to measure the parity-violating sign of the $\tau^- \rightarrow \nu_\tau W^-$ coupling (the tau neutrino helicity h_{ν_τ}).

More sophisticated models, such as the Isgur, Morningstar, Reader [12] flux-tube-breaking model, include D-wave $\rho\pi$, and K^*K threshold effects; these must be understood and taken into

account in order to accurately measure $h_{\nu\tau}$. They distort the mass-dependent width of the a_1 in measurable ways; these must be understood and taken into account in order to determine whether, *e.g.*, a radially excited a'_1 meson is present. Other models, such as the Unitarized Quark Model of Törnqvist [13], suggests the possibility that scalar mesons participate in the subsequent decay of the axial vector meson; if observed, this could give some insight into the properties of the (broad and thus poorly understood) scalar mesons. Contributions from *isoscalar* mesons such as the tensor f_2 and scalar f_0 would also produce non-trivial relations between the decay rates to $\pi^-\pi^+\pi^-$ and $\pi^-\pi^0\pi^0$.

Early work from ARGUS [14] saw significant D-wave $\rho\pi$ production, and hints of other contributions. Delphi '97 [15] saw anomalous substructure at high $M_{3\pi}$ — a hint of $a'_1(1700)$. Fig. 5 illustrates the potential complexity of this decay.



$$q = p_{\pi_1} - p_{\pi_{2/3}} \quad Q = p_{\pi_1} + p_{\pi_{2/3}} - p_{\pi_{3/2}} \quad P = p_{\pi_1} + p_{\pi_2} + p_{\pi_3}$$

Figure 5. Illustration of some of the many processes that can occur in the decay $\tau^- \rightarrow 3\pi\nu_\tau$.

3.1. $\tau \rightarrow 3\pi\nu_\tau$ decay rate

The decay rate can be described in terms of a matrix element squared $|\mathcal{M}|^2$ given by:

$$\text{Lepton Tensor} \times \text{Hadron Tensor} = \quad (9)$$

$$L_{\mu\nu} \times J^\mu J^{*\nu} = (S_{\mu\nu} + ih_{\nu\tau} A_{\mu\nu}) \times J^\mu J^{*\nu}, \quad (10)$$

where $S_{\mu\nu}$ is the symmetric part and $A_{\mu\nu}$ the anti-symmetric part of the lepton tensor, fully known in the Standard Model. The tau neutrino

helicity is given by $h_{\nu\tau} \equiv 2g_\nu g_a / (|g_\nu|^2 + |g_a|^2)$ which is -1 in the standard $V - A$ model. The hadronic current J^μ is a priori unknown, but can be parameterized in a model-dependent way, or in a model-independent way in terms of structure functions.

The Lorentz structure of J_μ is well-defined:

$$J_\mu = \left(-g_{\mu\nu} + \frac{P_\mu P_\nu}{P^2} \right) [(p_{\pi_1} - p_{\pi_2})^\nu F_1 + (p_{\pi_1} - p_{\pi_3})^\nu F_2 + (p_{\pi_2} - p_{\pi_3})^\nu F_3] + P_\mu F_4 \quad (11)$$

All the unknowns are in the form factors F_i , which are modeled in terms of Breit-Wigner functions for meson resonances, angular momentum factors (S,P,D...-wave), and potentially finite meson radius effects or other effects.

The overall tau decay rate and $s \equiv m^2(3\pi)$ spectrum is then given by

$$\begin{aligned} d\Gamma(\nu_\tau 3\pi) &= \frac{G_F^2 V_{ud}^2}{2m_\tau} [L^{\mu\nu} J_\mu J_\nu^*] dLips \quad (12) \\ &= \frac{G_F^2 V_{ud}^2}{32\pi^2 m_\tau} \left(1 + 2\frac{s}{m_\tau^2}\right) \left(1 - \frac{s}{m_\tau^2}\right) \\ &\quad \times |BW(s)|^2 \times \frac{\Gamma_{3\pi}(s)}{s} ds, \quad (13) \end{aligned}$$

where $BW(s)$ might be an overall Breit-Wigner line shape for the a_1 , and $\Gamma_{3\pi}(s)$ is the mass-dependent decay rate to 3π .

3.2. $h_{\nu\tau}$ from $\tau \rightarrow 3\pi\nu$

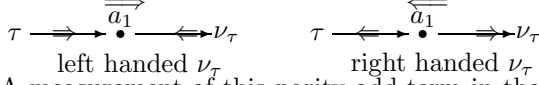
Kühn and Wagner pointed out in 1984 [11] that the parity-violating *signed* tau neutrino helicity $h_{\nu\tau}$ can be measured using the decay $\tau \rightarrow 3\pi\nu$, owing to its presence in Eqn. 10. This requires an asymmetric part of the hadron tensor $J^\mu J^{*\nu}$. At least three pseudoscalars in final state are needed, and an interference term between two amplitudes is needed.

There are two identical pions in this decay; thus, the ρ can be formed in two ways:

$$\begin{aligned} \tau^- \rightarrow a_1^- \nu_\tau & \quad \text{or} \quad a_1^- \nu_\tau \\ & \hookrightarrow \rho_1^0 \pi_2^- & \hookrightarrow \rho_1^0 \pi_1^- \\ & \hookrightarrow \pi_1^- \pi^+ & \hookrightarrow \pi_2^- \pi^+ \end{aligned} \quad (14)$$

The imaginary part of the interference term between these two amplitudes $\Im(BW(\rho_1) \cdot$

$BW(\rho_2)^*$ is a parity-odd observable that resolves the left- and right-handed part of the transverse polarization of the a_1 :



A measurement of this parity-odd term in the decay rate permits a measurement of $h_{\nu_{\tau}}$, so long as the parity-even (dominant) part of the decay rate is well and truly modeled.

3.3. CLEO results on $\tau \rightarrow 3\pi\nu_{\tau}$

CLEO has recently published two papers on our analysis of the $\tau^{-} \rightarrow \nu_{\tau}\pi^{-}\pi^0\pi^0$ decay. This decay is favored over the all-charged $\nu_{\tau}\pi^{-}\pi^{+}\pi^{-}$ decay, despite lower statistics, because of less background (from $K\pi\pi$, $KK\pi$, 4π , and hadronic events), and because isoscalar decays such as $f_2 \rightarrow \pi\pi$ have one entry per event in $a_1 \rightarrow \pi^{-}f_2 \rightarrow \pi^{-}\pi^0\pi^0$ but two in $\pi^{-}\pi^{+}\pi^{-}$.

In both papers, the full CLEO II sample of $\approx 4.3 \times 10^6$ $\tau^{+}\tau^{-}$ pairs was used, resulting in 30800 $\tau^{\mp} \rightarrow \pi^{\mp}\pi^0\pi^0\nu$ events (all tags), and 14600 $\tau^{\mp} \rightarrow \pi^{\mp}\pi^0\pi^0\nu$ lepton tagged events. The background is $\approx 10\%$, mostly $\tau \rightarrow 4\pi\nu$ and fake π^0 's.

The first paper [16] describes a model dependent analysis, in which the Dalitz plot distribution ($s_1 \equiv m^2(\pi^{-}\pi_1^0)$ vs $s_2 \equiv m^2(\pi^{-}\pi_2^0)$) is fitted, in bins of $s \equiv m^2(\pi^{-}\pi_1^0\pi_2^0)$, for contributions from different intermediate resonances and angular momenta. All measurable observables of production are also included in these fits. This results in a measured total width $\Gamma_{3\pi}(s) = \int J_{\mu}J^{*\mu}ds_1ds_2$. There is clear evidence for contributions from isoscalar intermediate resonances: $\sigma\pi$, $f_0\pi$, $f_2\pi$. There is also clear evidence of K^*K threshold turn-on in the $\Gamma_{3\pi}(s)$ mass dependence. In a second step, the overall lineshape $BW(s)$ is determined by measuring the invariant mass distribution of the three pions. In this paper, a measurement of the parity-violating signed neutrino helicity $h_{\nu_{\tau}}$, and model-dependent limits on scalar and vector 3π currents, are presented.

The second paper [17] describes a model independent analysis, in which the squared matrix element $|\mathcal{M}|^2$ is parameterized in terms of a sum

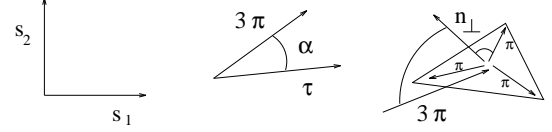


Figure 6. Kinematical variables characterizing the 3π system in $\tau \rightarrow 3\pi\nu_{\tau}$ decay: The Dalitz plot variables, and two angles that are measurable in the decay which are sensitive to its Lorentz structure.

of 16 independent terms [18]:

$$|\mathcal{M}|^2 = L_{\mu\nu} \times J^{\mu}J^{*\nu} = \sum_{X=1}^{16} L_X W_X, \quad (15)$$

where the L_X are 16 well-defined functions of decay observables, designed to select contributions to the overall hadronic current with different Lorentz structure (axial-vector, vector, scalar, *etc.*), and the W_X are 16 structure functions, functions of s , s_1 , and s_2 , that parameterize the hadronic dynamics. In this paper, model-independent limits on scalar and vector 3π currents are presented.

3.4. Model dependent analysis

In this analysis, the substructure in the hadronic current J^{μ} is determined in the context of a model, via a Likelihood fit to the Dalitz plot in full kinematical space, in bins of $m_{3\pi}$. The variables used are $s = m^2(3\pi)$, $s_1 = m^2(\pi^{-}\pi_1^0)$, $s_2 = m^2(\pi^{-}\pi_2^0)$; and the angular observables α , ψ defined in Fig. 6.

The amplitudes used in the fit to the 3π substructure which were found to be significant were:

- J_1^{μ} : s-wave $1^+ \rightarrow \rho\pi$
- J_2^{μ} : s-wave $1^+ \rightarrow \rho'\pi$
- J_3^{μ} : d-wave $1^+ \rightarrow \rho\pi$
- J_4^{μ} : d-wave $1^+ \rightarrow \rho'\pi$
- J_5^{μ} : p-wave $1^+ \rightarrow f_2(1275)\pi$

Table 2

Contributions to the total $\tau^- \rightarrow \pi^- \pi^0 \pi^0 \nu_\tau$ decay rate, and their significance.

		Significance	\mathcal{B} fraction(%)
ρ	s-wave		69.4
$\rho(1370)$	s-wave	1.4σ	$0.30 \pm 0.64 \pm 0.17$
ρ	d-wave	5.0σ	$0.36 \pm 0.17 \pm 0.06$
$\rho(1370)$	d-wave	3.1σ	$0.43 \pm 0.28 \pm 0.06$
$f_2(1275)$	p-wave	4.2σ	$0.14 \pm 0.06 \pm 0.02$
σ	p-wave	8.2σ	$16.18 \pm 3.85 \pm 1.28$
$f_0(1186)$	p-wave	5.4σ	$4.29 \pm 2.29 \pm 0.73$

- J_6^μ : p-wave $1^+ \rightarrow f_0(400 - 1200)\pi$, denoted as $\sigma\pi$
- J_7^μ : p-wave amplitude of $1^+ \rightarrow f_0(1370)\pi$

The mass and width of the $f_0(1370)$ and $f_0(400 - 1200)$ (σ) were fixed according to Törnqvist's Unitarized Quark Model [13]:

$$\begin{aligned} m_{f_0(1370)} &= 1.186 \text{ GeV}/c^2; \\ \Gamma_{f_0(1370)} &= 0.350 \text{ GeV}; \\ m_\sigma &= 0.860 \text{ GeV}/c^2; \\ \Gamma_\sigma &= 0.880 \text{ GeV}. \end{aligned}$$

The total current was parameterized as a coherent sum of these contributions:

$$J^\mu = \sum_{i=1}^{i=7} \beta_i \times J_i^\mu \times F_i, \quad (16)$$

where the β_i are (complex) fit parameters, and the F_i are form factors to take into account the finite size of the mesons involved: $F_i = e^{-0.5R^2 p_i^2}$. In the nominal fit, R was fixed at 0 (so that $F_i = 1$); in other fits, R was allowed to vary.

The results of these fits are illustrated in Fig. 7 and 8. Good fits ($< 3\sigma$) are obtained in all $m_{3\pi}$ bins. There is clear evidence in the s_3 projections at high s for the isoscalar $f_2(1275)$. The fit results for the various contributions to the total $\tau^- \rightarrow \pi^- \pi^0 \pi^0 \nu_\tau$ decay rate are given in Table 2.

We note that the $\rho\pi$ s-wave with $\mathcal{B} \approx 70\%$ is dominant, as expected. With the exception of $\rho'\pi$ s-wave, all amplitudes are significant; the K&S model is too simple. Isoscalars contribute to the 3π hadronic current with $\mathcal{B} \approx 20\%$; especially the σ cannot be neglected. Curiously, the ρ' shows up

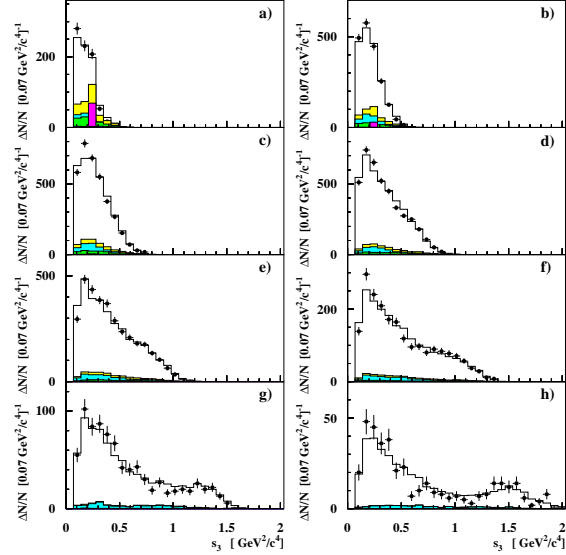


Figure 7. Results of the fit to the 3π substructure in $\tau^\mp \rightarrow \pi^\mp \pi_1^0 \pi_2^0 \nu_\tau$ decays. Shown are projections of the data and the fit in $s_3 = m_{\pi_1^0 \pi_2^0}^2$. In each plot, the points with error bars are the data, and the histograms are the results of the fit. The plots are for different values of $m_{3\pi}$: (a) 0.6 – 0.9 GeV; (b) 0.9 – 1.0; (c) 1.0 – 1.1; (d) 1.1 – 1.2; (e) 1.2 – 1.3; (f) 1.3 – 1.4; (g) 1.4 – 1.5; (h) 1.5 – 1.8.

more strongly in d-wave than in s-wave. Finally, the couplings to each of the J_i sub-currents are consistent with being constant as a function of $m_{3\pi}$, suggesting that only one resonance (the a_1) is responsible for all this substructure.

There is no evidence for scalar 3π currents, and the following model-dependent upper limits at 90% CL are derived:

$$\mathcal{B}(\tau \rightarrow \pi' \nu \rightarrow \rho \pi \nu \rightarrow 3\pi \nu) < 1.0 \times 10^{-4} \quad (17)$$

$$\mathcal{B}(\tau \rightarrow \pi' \nu \rightarrow \sigma \pi \nu \rightarrow 3\pi \nu) < 1.9 \times 10^{-4} \quad (18)$$

$$h_{\nu_\tau} = -1.02 \pm 0.13 \pm 0.03 \text{ (SM} = -1) \quad (19)$$

These fit results can be converted to a model for the all charged mode, $\tau^\mp \rightarrow \pi^\mp \pi^\mp \pi^\pm \nu$. The

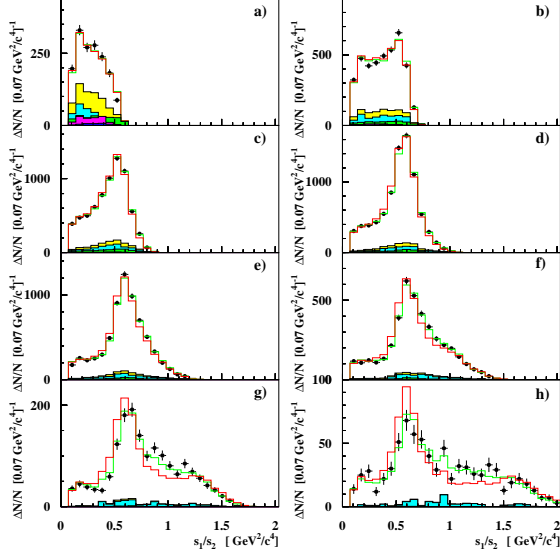


Figure 8. Results of the fit to the 3π substructure in $\tau^\mp \rightarrow \pi^\mp \pi_1^0 \pi_2^0 \nu_\tau$ decays. Shown are projections of the data and the fit in $s_1 = m_{\pi^- + \pi_1^0}^2$ and $s_2 = m_{\pi^- + \pi_2^0}^2$ (two entries per event). In each plot, the points with error bars are the data, filled histograms are background contributions, and the clear histograms are the results of the fit. The plots are for different values of $m_{3\pi}$, as in Fig. 7.

conversion is non-trivial, due to the presence of isoscalars with different isospin structure:

$$\begin{aligned}
 |0, 0\rangle &= \frac{1}{\sqrt{3}} |1, +1\rangle |1, -1\rangle \\
 &+ \frac{1}{\sqrt{3}} |1, -1\rangle |1, +1\rangle - \frac{1}{\sqrt{3}} |1, 0\rangle |1, 0\rangle.
 \end{aligned} \quad (20)$$

Although this fit procedure was not applied to the ≈ 80000 $\tau^\mp \rightarrow \pi^\mp \pi^\mp \pi^\pm \nu$ events selected from the CLEO data set, qualitative agreement with the Dalitz plot distributions is excellent. In addition, the total decay rate predicted for $\tau^\mp \rightarrow \pi^\mp \pi^\mp \pi^\pm \nu$ is in excellent agreement with the world average measured values [8].

To model the full three pion mass spectrum, we form a coherent superposition of contributions

from the a_1 and a radially excited a_1' :

$$\begin{aligned}
 B(s) &= B_{a_1}(s) + \kappa \cdot B_{a_1'}(s) \\
 &= \frac{1}{s - m_{a_1}^2(s) + im_{0a_1} \Gamma_{tot}^{a_1}(s)} \\
 &+ \frac{\kappa}{s - m_{0a_1'}^2 + im_{0a_1'} \Gamma_{tot}^{a_1'}(s)}.
 \end{aligned} \quad (21)$$

The total width $\Gamma_{tot}(s)$ must be modeled carefully. We integrate the fit results for J^μ over the Dalitz plot in bins of $m(3\pi)$, and include contributions to the total width from $K^*K \rightarrow KK\pi$ and $f_0(980)\pi \rightarrow KK\pi$:

$$\begin{aligned}
 \Gamma_{tot}(s) &= \Gamma_{2\pi^0\pi^-}(s) + \Gamma_{2\pi^-\pi^+}(s) \\
 &+ \Gamma_{K^*K}(s) + \Gamma_{f_0(980)\pi}(s)
 \end{aligned} \quad (23)$$

If the total width runs (is a function of s), then the mass $m^2(s)$ can run as well:

$$m^2(s) = m_0^2 + \frac{1}{\pi} \int_{s_{th}}^{\infty} \frac{m_0 \Gamma_{tot}(s')}{(s - s')} ds' \quad (24)$$

Thus we perform χ^2 fits to the total $m(3\pi)$ spectrum with and without a_1' ; with $KK\pi$ contributions to Γ_{tot} or not; with running mass or constant mass; and with or without finite meson radii.

We obtain good fits with either constant or running mass, with and without $f_0(980)\pi$, and for meson radii anywhere in the range $0 \leq R \leq 2 \text{ GeV}^{-1}$. The K^*K threshold is needed for good fit. The best fits are obtained for R in the range $1.2 \leq R \leq 1.4 \text{ GeV}^{-1}$. Our nominal fit is chosen as the one with constant a_1 mass, K^*K threshold included, no $f_0(980)\pi$ threshold, and $R = 0$. The fit results are shown in Fig. 9. We obtain $m_{a_1} = 1.331 \pm 0.010 \pm 0.003$, $\Gamma_{a_1} = 0.814 \pm 0.036 \pm 0.013$, $\mathcal{B}(a_1 \rightarrow K^*K) = (3.3 \pm 0.5 \pm 0.1)\%$, with a $\chi^2 = 39.3/41$ dof. Here, again, we observe consistent results with the all-charged mode $\tau^- \rightarrow \pi^- \pi^+ \pi^- \nu_\tau$.

It is important to note that the parameters of the a_1 resulting from this fit have a large model dependence, which is not included in the systematic errors. These parameters will change if additional, higher-mass contributions are added to the fit.

There appears to be a small excess of data at high s , suggesting the presence of an a_1'

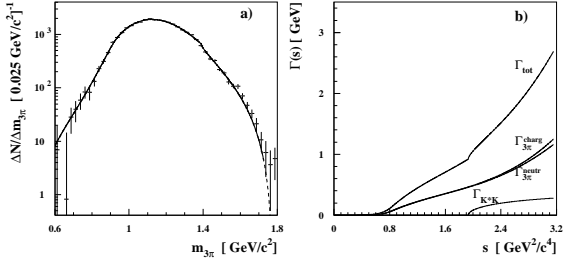


Figure 9. (a) Nominal fit to the $m(3\pi)$ spectrum with no a'_1 . Points with errors are the data; solid line is the fit result. Note the kink around $m_{3\pi} = 1.4$ GeV due to the turn-on of the K^*K threshold in the total width. (b) Calculated contributions to the total width $\Gamma_{3\pi}(s)$.

and/or more thresholds in the total width. We have therefore performed a fit including the a'_1 , as in Eqn. 22. We are not sensitive to the mass or width of the a'_1 , and thus fix them to be $m_{a'_1} = 1700$ MeV, $\Gamma_{a'_1} = 300$ MeV. The fit results are shown in Fig. 10. We obtain $|\kappa| = 0.053 \pm 0.019$ (stat.) with phase ϕ_κ consistent with zero, and $\chi^2 = 28.9/39$ dof. The improvement of fit yields a significance of 2.9σ for the a'_1 , and $\mathcal{B}(\tau \rightarrow a'_1 \nu) = (1.6 \pm 1.1 \pm 0.3 \pm 0.7) \times 10^{-4}$. More statistics needed to conclusively state if the a'_1 participates or not in $\tau \rightarrow 3\pi\nu$ decay.

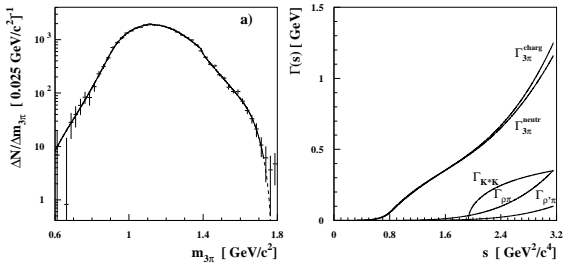


Figure 10. Fit to the $m(3\pi)$ spectrum including the a'_1 . See caption to Fig. 9.

Table 3

Composition of the structure functions in terms of the spin and parity J^P of the hadronic current.

	$J = 0$ h^0	$J^P = 1^+$ h^1, h^2	$J^P = 1^-$ h^3
$J = 0$ h^{*0}	\mathbf{W}_{SA}		
$J^P = 1^+$ h^{*1}, h^{*2}	W_{SB}, W_{SC}	\mathbf{W}_A	
$J^P = 1^-$ h^{*3}	W_{SD}, W_{SE}	W_C, W_D, W_E	\mathbf{W}_B
	W_{SF}, W_{SG}	W_F, W_G	W_H, W_I

3.5. $\tau \rightarrow 3\pi\nu_\tau$ Structure functions

CLEO has analyzed its 14600 $\tau^\mp \rightarrow \pi^\mp \pi^0 \pi^0 \nu$ lepton tagged events in terms of the structure functions defined in Ref. [18]. The decay rate is written as:

$$d\Gamma_{3\pi\nu_\tau} \propto \sum_X^{16} \bar{L}_X(\alpha, \beta, \gamma) W_X(s, s_1, s_2) d\text{Phs} \quad (25)$$

$$\text{with } X \in \{A, B, \dots, I, SA, SB, \dots, SG\}. \quad (26)$$

The 16 structure functions W_X that contain all the information on the hadronic structure depend on s , s_1 , and s_2 only. We can measure these structure functions independent of any model. They can be interpreted by comparing them with predictions from a model for J^μ , such as the one resulting from the fit described above.

In the 3π rest frame, with z -axis perpendicular to the 3π decay frame, the hadronic current h^μ has a time-like component h^0 from pseudoscalar currents (such as the π'), a component along the z axis, h^3 , from vector currents (such as $\rho' \rightarrow \rho\pi$ via the Wess-Zumino anomaly), and transverse components h^1 and h^2 from the dominant axial-vector current (such as the a_1). The leptonic tensor components L_X are defined so as to decompose the hadronic current into contributions from the different J^P -states (scalar, vector, axial) according to Table 3. The measurement of the structure functions W_{SA} and W_B allows us to determine the non-axial vector contributions model independently. More directly, we can look for non-zero contributions to the real or imaginary parts of h^0 or h^3 in bins of s , s_1 , and s_2 .

The structure functions $W_A(s)$, $W_C(s)$, $W_D(s)$, and $W_E(s)$ remain non-zero when one integrates over the Dalitz plot variables s_1 and s_2 . Their measured distribution is shown in Fig. 11. The data are compared with the K&S model and with the results of the CLEO fit to the more elaborate model described above.

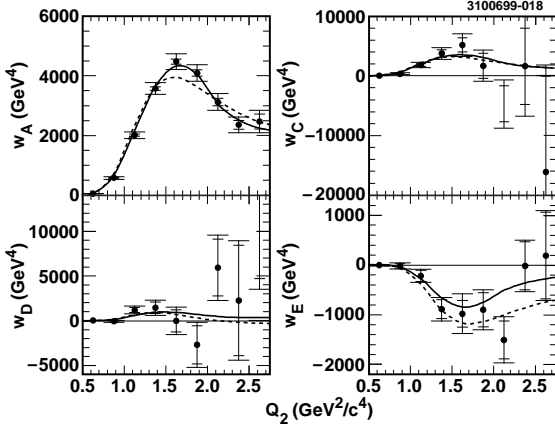


Figure 11. The structure functions $W_A(s)$, $W_C(s)$, $W_D(s)$, and $W_E(s)$ integrated over s_1 and s_2 , as measured by CLEO. The dashed line is the prediction from the K&S model, and the solid line is the prediction from the CLEO model-dependent fit.

The components of the hadronic current h^μ as described above can be measured in the full s , s_1 , and s_2 space. Choosing a set of bins in this 3D space as described in Ref. [17], we obtain the results shown in Figs. 12 and 13. The axial-vector induced components of the hadronic current are well described by the CLEO model-dependent fit, while the non-axial-vector components are consistent with zero everywhere. From this, we extract a model-independent limits on scalar and vector contributions to the $\tau^- \rightarrow 3\pi\nu_\tau$ decay, at 95% CL:

$$\mathcal{B}(\tau^\mp \rightarrow S\nu \rightarrow (3\pi)^\mp\nu)/\mathcal{B}(\tau^\mp \rightarrow (3\pi)^\mp\nu) < 9.4\%(27)$$

$$\mathcal{B}(\tau^\mp \rightarrow V\nu \rightarrow (3\pi)^\mp\nu)/\mathcal{B}(\tau^\mp \rightarrow (3\pi)^\mp\nu) < 7.3\%(28)$$

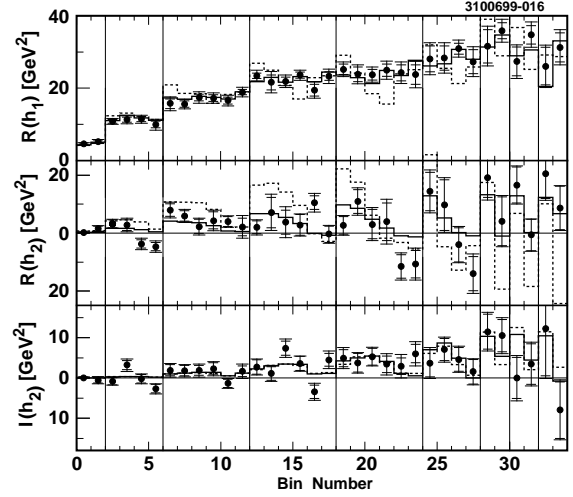


Figure 12. The real and imaginary parts of the 3π hadron current induced by axial vector current, as measured by CLEO. Dashed line is the prediction from the K&S model, and the solid line is the prediction from the CLEO model-dependent fit.

From the measured hadronic current, all sixteen structure functions in the $\tau^- \rightarrow 3\pi\nu_\tau$ decay have been determined, for the first time.

3.6. Summary on $\tau \rightarrow 3\pi\nu_\tau$

The high statistics CLEO analyses of $\tau \rightarrow 3\pi\nu_\tau$ are permitting detailed studies of the hadronic substructure, precision measurements of signed ν_τ helicity, and have revealed significant contributions to the 3π system other than $a_1 \rightarrow \rho\pi$. The model-dependent fits to full kinematical distribution reveal significant signals for isoscalars (f_0 , f_2 , and σ), clear evidence for K^*K threshold, weak evidence for a_1' , and limits on the PCAC-violating π' . The model-independent structure function analyses give limits on non axial vector contributions, and clean tests of the models. Still, there are many open questions: Can we learn more about the a_1 lineshape: running/constant mass, thresholds, *etc.*? Is there an a_1' ? How does it decay? Are there other components to the

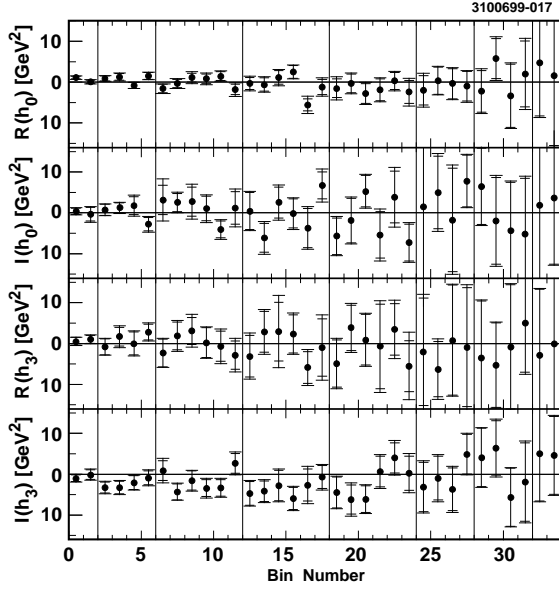


Figure 13. The real and imaginary parts of the 3π hadron current induced by the scalar (h^0) and vector (h^3) currents, as measured by CLEO.

substructure? A detailed analysis of the higher-statistics all-charged $\tau^- \rightarrow \pi^- \pi^+ \pi^- \nu_\tau$ mode may shed more light on these questions.

4. $\tau^- \rightarrow (4\pi)^- \nu_\tau$

We expect the $\tau \rightarrow 4\pi \nu_\tau$ decay to proceed via the vector ($J^P = 1^-$) current, dominated by the ρ meson and its radial excitations ρ' , ρ'' , etc.. Axial vector currents are “second-class” (isospin violating); an example is $\tau \rightarrow b_1 \nu_\tau$, $b_1 \rightarrow \omega \pi$. Given the large phase space for the 4π system, even the simplest models are already complicated!

CLEO has analyzed these decays with the goals of extracting the parameters (mass and pole width) of the ρ' ; searching for second class (axial) currents; exploring the resonant decomposition of 4π system ($\omega \pi$, $\eta \pi$, $a_1 \pi$); and testing CVC by comparing the cross sections for $e^+ e^- \rightarrow 2\pi^+ 2\pi^-$, $\pi^+ \pi^- 2\pi^0$ at low energy to $\tau^- \rightarrow \nu_\tau 2\pi^- \pi^+ \pi^0$, $\pi^- 3\pi^0$.

A good model of the 4π spectral function is needed in order to reliably extract a limit on the tau neutrino mass from the 4π kinematical distributions. CLEO [19] set the limit $m_{\nu_\tau} < 28$ MeV/ c^2 , 95% CL; the 4 MeV model-dependence dominates the systematic error in that measurement.

The decay $\tau \rightarrow \omega \pi \nu$ first measured by ARGUS [20] and CLEO [21] in 1987. The $\rho \pi \pi$ branching fractions were measured by ARGUS [22] in 1991, and ALEPH in 1997 [23]. The mass and width of ρ' were extracted from $\tau \rightarrow \pi \pi^0 \nu$ by ALEPH in 1997 [7] and CLEO in 1999 [3].

4.1. $\tau \rightarrow 4\pi \nu_\tau$ from CLEO

The CLEO analysis [24] uses the CLEO-II data set of $N_{\tau\tau} \approx 4.3 \times 10^6$ produced tau pairs, and selects $\sim 24,000$ events consistent with $\tau^\mp \rightarrow \pi^\mp \pi^\pm \pi^\mp \pi^0 \nu_\tau$. The $m(4\pi)$ mass spectrum is shown in Fig. 14. After subtracting estimated backgrounds dominated by $K \pi \pi \pi \nu$, $KK \pi \pi \nu$, $K_S \pi \pi \nu$, we extract the branching fraction

$$\mathcal{B}(\tau^- \rightarrow 3\pi \pi^0 \nu_\tau) = (4.19 \pm 0.10 \pm 0.21)\%. \quad (29)$$

4.2. $\omega \pi$ Spectral Function

We construct the spectral function $V^{3\pi\pi^0}(q)$, $q = m(3\pi\pi^0)$ by correcting for background, efficiency, and the production dynamics:

$$V^{3\pi\pi^0}(q) = \frac{1}{N} \frac{dN(q)}{dq} \frac{1}{q(M_\tau^2 - q^2)^2 (M_\tau^2 + 2q^2)} \times \frac{\mathcal{B}(\tau \rightarrow 3\pi \pi^0 \nu_\tau)}{\mathcal{B}(\tau \rightarrow e \nu_e \nu_\tau)} \frac{M_\tau^8}{12\pi V_{ud}^2}. \quad (30)$$

Focusing on $\tau^\mp \rightarrow \omega \pi^\mp \nu_\tau$, we extract the ω signal in bins of $q = M(3\pi\pi^0)$, and form the $V^{\omega\pi}(q)$ spectral function, and the remainder:

$$V^{non-\omega\pi}(q) \equiv V^{3\pi\pi^0}(q) - V^{\omega\pi}(q). \quad (31)$$

These are shown in Fig. 15.

We fit the $\omega \pi$ spectral function using a coherent sum of combinations of Breit-Wigner lineshapes with mass dependent widths, for $\rho(770)$, ρ' , and $\rho''(1700)$. We take the parameters of the ρ and ρ'' as known:

$$M_\rho = 770 \text{ MeV}/c^2; \quad \Gamma_\rho = 151 \text{ MeV}/c^2; \quad (32)$$

$$M_{\rho''} = 1700 \text{ MeV}/c^2; \quad \Gamma_{\rho''} = 235 \text{ MeV}/c^2. \quad (33)$$

The results of these fits are shown in Fig. 16.

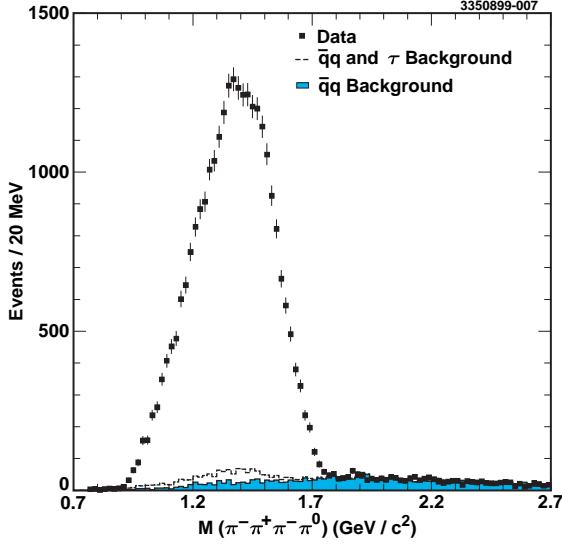


Figure 14. The $m(4\pi)$ mass spectrum in $\tau^\mp \rightarrow \pi^\mp \pi^\pm \pi^\mp \pi^0 \nu_\tau$ as measured by CLEO, before background subtraction.

Good fits are obtained only when both the $\rho(770)$ and $\rho(1450)$ are included. Results with the $\rho'(1700)$ included or not included give consistent results for the ρ' parameters:

$$M_{\rho'} = (1.523 \pm 0.010) \text{ GeV}/c^2 \quad (34)$$

$$\Gamma_{\rho'} = (0.400 \pm 0.035) \text{ GeV}/c^2. \quad (35)$$

Recall from the 2π channel, we had $M_{\rho'} \sim 1400$ MeV. The PDG values are

$$M_{\rho'} = (1.465 \pm 0.025) \text{ GeV}/c^2, \quad (36)$$

$$\Gamma_{\rho'} = (0.310 \pm 0.060) \text{ GeV}/c^2, \quad (37)$$

dominated by proton experiments on fixed target, $e^+e^- \rightarrow \pi^+\pi^-$ and $e^+e^- \rightarrow \eta\pi^+\pi^-$, as well as from earlier $\tau \rightarrow \pi\pi^0\nu$ results. The origin of these differences is unresolved.

4.3. Second Class Currents in $\tau \rightarrow \omega\pi\nu$

There are two axial-vector ($J^P = 1^+$) states: The $a_1(1260)$ in the 3P_1 octet, with $J^{PG} = 1^{+-}$, couples to the W as a “first-class” current; the

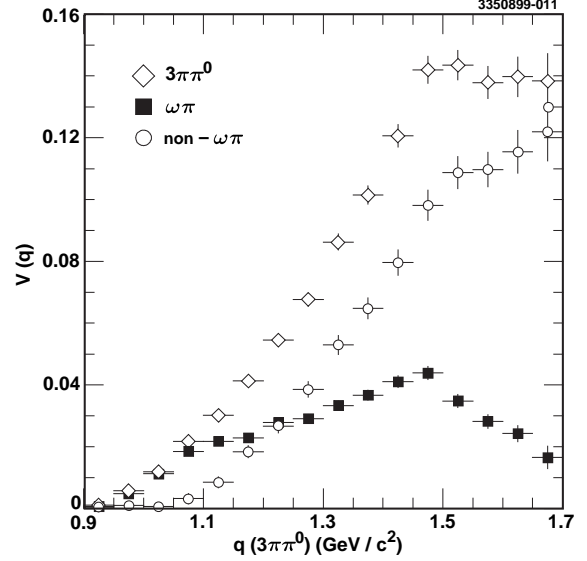


Figure 15. The spectral functions in bins of $q = M(3\pi\pi^0)$ as measured by CLEO: the total $V^{3\pi\pi^0}(q)$ (open diamonds), $V^{\omega\pi}(q)$ (filled squares), and $V^{\text{non-}\omega\pi}(q)$ (open circles).

$b_1(1235)$ in the 1P_1 octet, with $J^{PG} = 1^{++}$, doesn't couple to the W (“second-class” current) except via isospin (G-parity) violation (the weak decay constant $f_{b_1} \approx 0$).

The a_1 decays to $\rho\pi$ via S-wave, thence to 3π . The ρ' decays to $\omega\pi$ via P-wave, thence to 4π . The b_1 decays to $\omega\pi$ via S-wave, thence to 4π . The difference in G-parity for the states which decay to 4π is reflected in the different expected polarization of the ω meson, and thus in the angular distribution of the angle between the normal to the ω decay plane and the direction of the 4th pion (“helicity angle”) $\cos \chi = \hat{n}_\perp^\omega \cdot \hat{p}_{\pi_4}$. The different expected angular distributions are given in Table 4.

The fit to the $\cos \chi$ distribution for the CLEO $\tau \rightarrow \omega\pi\nu_\tau$ data (corrected for background and efficiency) is shown in Fig. 17. There is no evidence for non-vector current contributions, and CLEO

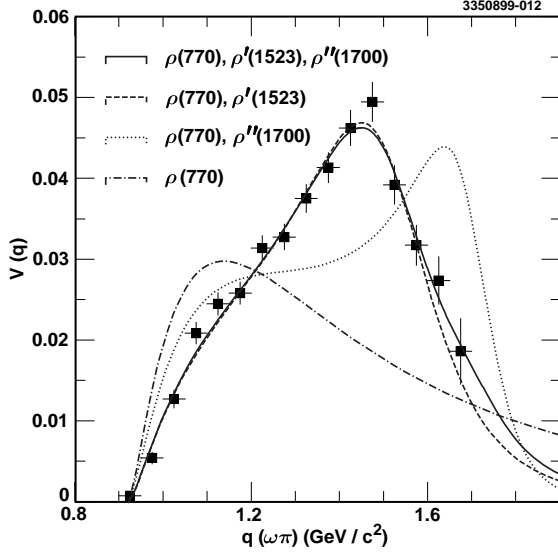


Figure 16. Fits to the $V^{\omega\pi}(q)$ spectral function measured by CLEO in $\tau \rightarrow \omega\pi\nu_\tau$.

sets the limit

$$N^{\omega\pi}(\text{non-vec})/N^{\omega\pi}(\text{vector}) < 6.4\% \quad (38)$$

at 95% CL, to be compared with ALEPH's limit [23] of $< 8.6\%$.

4.4. $\tau \rightarrow 3\pi\pi^0\nu$ resonant structure

We perform an unbinned maximum likelihood fit in the full kinematical space of the $\tau \rightarrow 3\pi\pi^0\nu$ decay, to extract a model-dependent description of its resonant structure. We use the structure function approach to describe the production of

Table 4

Expected distributions of the ω helicity angle χ in $\tau \rightarrow \omega\pi\nu_\tau$.

J^P	L	$F(\cos\chi)$
1^-	1	$1 - \cos^2\chi$
1^+	0	1
1^+	2	$1 + 3\cos^2\chi$
0^-	1	$\cos^2\chi$

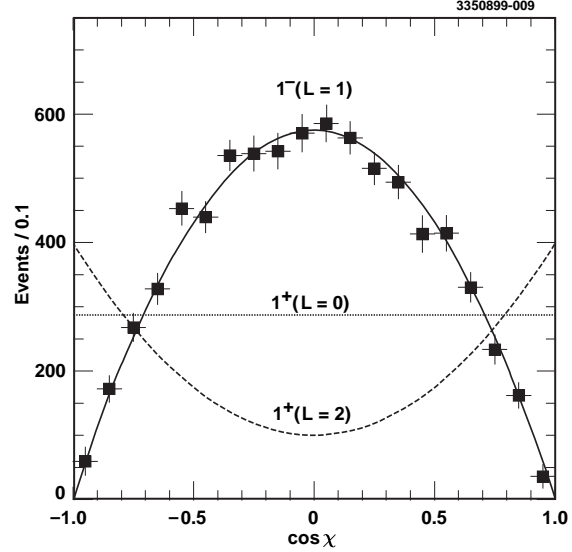


Figure 17. Fit to the $\cos\chi$ distribution for the CLEO $\tau \rightarrow \omega\pi\nu_\tau$ data. Black squares are the data, lines are the predictions for the different J^P contributions.

the 4π system from tau decay, averaging over the unseen neutrino:

$$|\mathcal{M}|^2 = \frac{G_F^2}{2} V_{ud}^2 L^{\mu\nu} J_\mu J_\nu^*, \quad (39)$$

$$f_S = \overline{L^{\mu\nu} J_\mu J_\nu^*} = 2(M_\tau^2 - q^2) \sum_{i=1}^{16} \overline{L_i} W_i. \quad (40)$$

The hadronic current J^μ is modeled in terms of resonances:

$$J^\mu = \alpha_\omega f_\omega^\mu F_\omega(q) + \sum_k \alpha_k f_k^\mu F_k(q), \quad (41)$$

$$F_k(q) = \beta_k^0 + \beta_k BW_\rho(q) + \beta_k' BW_{\rho'}(q) + \beta_k'' BW_{\rho''}(q), \quad (42)$$

where k runs over substructure components of the model (see below). The α 's and β 's are fit parameters. The background PDF is modeled using an empirical form derived from the CLEO data.

Four models were tried:

- Model 1: $\omega\pi$, $\rho\pi\pi$ and non-resonant $3\pi\pi^0$;
- Model 2: $\omega\pi$ and $a_1\pi$;
- Model 3: $\omega\pi$, $a_1\pi$, $\sigma\rho$ and $f_0(980)\rho$;
- Model 4: $\omega\pi$, $a_1\pi$ and $\rho\pi\pi$.

The projections of the data, and the results of the fit to Model 2, are shown in Fig. 18. There is clear evidence for contributions from $\omega\pi^-$, $\rho^0\pi^-\pi^0$, $\rho^-\pi^+\pi^-$, and $\rho^+\pi^-\pi^-$. The CLEO data prefer models containing at least $\omega\pi$ and $a_1\pi$, in good agreement with results from the CMD-2 analysis [25] of $e^+e^- \rightarrow 4\pi$. The data do not rule out small contributions from modes like $\sigma\rho$, $f_0\rho$, or non-resonant $\rho\pi\pi$.

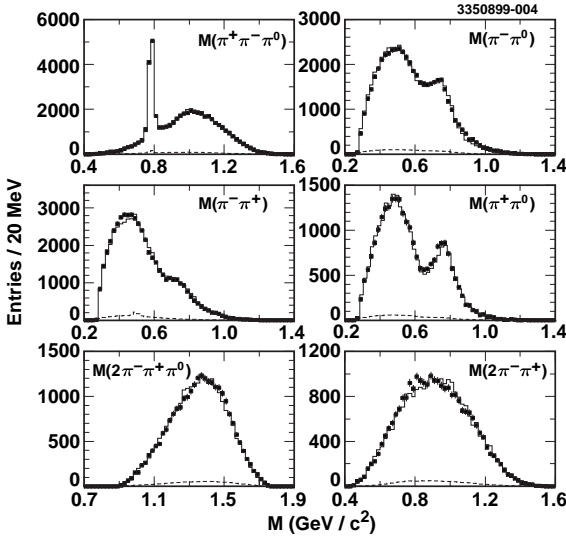


Figure 18. Mass and sub-mass distributions in $\tau \rightarrow 3\pi\pi^0\nu$ decays as measured by CLEO (data points). The histograms are the results of a fit in the full kinematical space of this decay, using Model 2 as described in the text.

4.5. Test of CVC in 4π

As a test of CVC, we can compare the 4π and $\omega\pi$ spectral functions measured in $\tau \rightarrow 4\pi\nu_\tau$

charged current decays with the analogous ones measured (by CMD-2 [25]) in e^+e^- annihilation via the neutral EM current:

$$V^{3\pi\pi^0}(q) = \frac{q^2}{4\pi^2\alpha^2} \left[\frac{1}{2}\sigma_{e^+e^- \rightarrow 2\pi^+2\pi^-}(q) + \sigma_{e^+e^- \rightarrow \pi^+\pi^-2\pi^0}(q) \right]; \quad (43)$$

$$V^{\omega\pi}(q) = \frac{q^2}{4\pi^2\alpha^2} \sigma_{e^+e^- \rightarrow \omega\pi^0}(q). \quad (44)$$

This is done in Fig. 19.

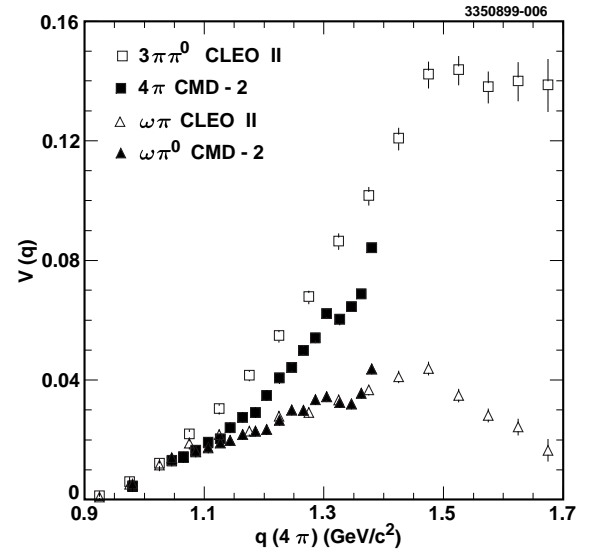


Figure 19. Comparison of the 4π and $\omega\pi$ spectral functions measured (by CLEO) in $\tau \rightarrow 4\pi\nu_\tau$ decays with the analogous ones measured (by CMD-2 [25]) in e^+e^- annihilation.

The CMD-2 data, which include a 15% systematic error on the overall normalization, show clear dominance of $a_1\pi$ and $\omega\pi$ in $e^+e^- \rightarrow 4\pi$. We see that the shapes agree well between τ and e^+e^- data. However, the normalization of the 4π (non- $\omega\pi$) spectral functions do not agree with one another. This is also seen in the total branching fraction for $\tau \rightarrow 3\pi\pi^0\nu$ predicted [9] from the

(pre-CMD-2) e^+e^- data using CVC:

$$B(\tau \rightarrow 3\pi\pi^0\nu) = (4.22 \pm 0.10)\% \quad (45)$$

$$CVC(\text{excl. CMD} - 2) : (4.06 \pm 0.25)\%. \quad (46)$$

This disagreement might be due to normalization errors, other experimental errors, or a real violation of CVC.

5. 5π , 6π , 7π

The decays of the τ to $5\pi\nu$, $6\pi\nu$, and $\geq 7\pi\nu$ all have small branching fractions:

$$\mathcal{B}(2\pi^-\pi^+2\pi^0\nu_\tau) = (5.3 \pm 0.4) \times 10^{-3} \quad (47)$$

$$\mathcal{B}(3\pi^-\pi^+2\pi^0\nu_\tau) = (7.8 \pm 0.6) \times 10^{-4} \quad (48)$$

$$\mathcal{B}(2\pi^-\pi^+3\pi^0\nu_\tau) = (2.9 \pm 0.8) \times 10^{-4} \quad (49)$$

$$\mathcal{B}(3\pi^-\pi^+2\pi^0\nu_\tau) = (2.2 \pm 0.5) \times 10^{-4} \quad (50)$$

$$\mathcal{B}(3\pi^-\pi^+2\pi^0\nu_\tau) < 1.1 \times 10^{-4} \quad (51)$$

$$\mathcal{B}(7\pi^\pm(\pi^0)\nu_\tau) < 2.4 \times 10^{-6}. \quad (52)$$

The limits on $\geq 7\pi\nu$ come from CLEO [26]. CLEO has no new results on 5π modes, but there are new results from CLEO [27] on $2\pi^-\pi^+3\pi^0$ and $3\pi^-\pi^+2\pi^0$.

The decays $\tau^- \rightarrow (6\pi)^-\nu_\tau$ have three modes:

- $\tau^- \rightarrow 3\pi^-\pi^+\pi^0\nu_\tau$
- $\tau^- \rightarrow 2\pi^-\pi^+3\pi^0\nu_\tau$
- $\tau^- \rightarrow \pi^-5\pi^0\nu_\tau$

The mode $\tau^- \rightarrow \pi^-5\pi^0\nu_\tau$ has low efficiency and large combinatoric background; CLEO has no signal or results on this mode.

These decays all have very complex substructure. We expect significant resonant substructure (ρ 's, ω 's, η 's). We expect the $(6\pi)^-$ system to be dominantly produced via the vector current, although there can be axial vector current contributions from $(3\pi)^-\eta$, $\eta \rightarrow 3\pi$.

From data on the $I = 1$ component of $e^+e^- \rightarrow 6\pi$, CVC predicts [28]

$$v_1^{6\pi}(q^2) = \frac{q^2}{4\pi^2\alpha^2}\sigma_{I=1}(e^+e^- \rightarrow 6\pi), \quad (53)$$

$$\mathcal{B}(\tau^- \rightarrow (6\pi)^-\nu_\tau) \geq (1.23 \pm 0.19) \times 10^{-3}. \quad (54)$$

5.1. Isospin in $\tau^- \rightarrow (6\pi)^-\nu_\tau$

As a first step in describing the resonant substructure in 6π states, we can classify them by their isospin content, with ‘‘partitions’’ (triplets of numbers n_1, n_2, n_3):

n_3 = number of 3π isoscalar systems (ω),

$n_2 - n_3$ = number of 2π isovector systems (ρ),

$n_1 - n_2$ = number of π isovector systems.

For example, $(3, 2, 1) = (\pi\rho\omega)$. The contributions of each partition to final states are given by:

$$\Gamma(\pi^-5\pi^0) = \frac{9}{35}\Gamma(4\pi\rho) \quad (55)$$

$$\Gamma(2\pi^-\pi^+3\pi^0) = \frac{2}{7}\Gamma(4\pi\rho) + \frac{1}{5}\Gamma(3\pi\omega) + \frac{4}{5}\Gamma(3\rho) + \frac{1}{2}\Gamma(\pi\rho\omega) \quad (56)$$

$$\Gamma(3\pi^-\pi^+2\pi^0) = \frac{16}{35}\Gamma(4\pi\rho) + \frac{4}{5}\Gamma(3\pi\omega) + \frac{1}{5}\Gamma(3\rho) + \frac{1}{2}\Gamma(\pi\rho\omega). \quad (57)$$

Isospin conservation constrains the partial rates

$$f(2\pi^-\pi^+3\pi^0) = \Gamma(2\pi^-\pi^+3\pi^0)/\Gamma(6\pi) \quad (58)$$

$$f(3\pi^-\pi^+2\pi^0) = \Gamma(3\pi^-\pi^+2\pi^0)/\Gamma(6\pi) \quad (59)$$

$$f(\pi^-5\pi^0) = 1 - f(2\pi^-\pi^+3\pi^0) - f(3\pi^-\pi^+2\pi^0) \quad (60)$$

to lie inside the space illustrated in Fig. 20. CLEO can measure only the ratio $f(2\pi^-\pi^+3\pi^0)/f(3\pi^-\pi^+2\pi^0)$.

Axial vector currents can produce 6π final states, due primarily (one assumes) to intermediate states $(3\pi)^-\eta$, $\eta \rightarrow 3\pi$. Two mechanisms have been proposed to predict the rate for these decays. A G-parity violating term, suppressed by $(m_u^2 - m_d^2)/(m_u^2 + m_d^2)$ yields the prediction [29]

$$\mathcal{B}(\pi^-2\pi^0\eta\nu_\tau) \simeq \mathcal{B}(2\pi^-\pi^+\eta\nu_\tau) \simeq 1.2 \times 10^{-6}. \quad (61)$$

An anomalous Wess-Zumino term without $(m_u^2 - m_d^2)$ suppression yields the predictions [30]

$$\mathcal{B}(f_1\pi^-\nu_\tau) = 2.9 \times 10^{-4} \quad (62)$$

$$\mathcal{B}(\pi^-\rho^0\eta\nu_\tau \rightarrow 2\pi^-\pi^+\eta\nu_\tau) = 2.9 \times 10^{-4} \quad (63)$$

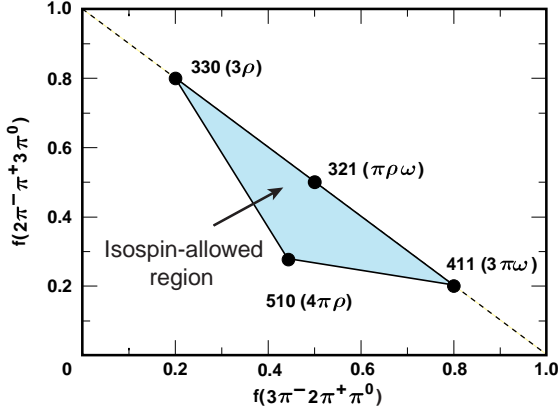


Figure 20. Isospin-allowed region in the space of 6π partial rate fractions, as described in the text.

5.2. CLEO results for $\tau^- \rightarrow 6\pi\nu_\tau$

Using the full CLEO II and CLEO II.V data set, corresponding to 12.3×10^6 produced $\tau^+\tau^-$ pairs, we reconstruct (139 ± 12) events in the mode $\tau^- \rightarrow 2\pi^-\pi^+3\pi^0\nu_\tau$, with a background of 36% from other tau decays and from hadronic events. The 6π mass spectrum is shown in Fig. 21. We measure [27] a branching fraction

$$\mathcal{B}(2\pi^-\pi^+3\pi^0\nu_\tau) = (2.2 \pm 0.3 \pm 0.4) \times 10^{-4}. \quad (64)$$

We reconstruct (231 ± 19) events in the mode $\tau^- \rightarrow 3\pi^-2\pi^+\pi^0\nu_\tau$, with a background of 20% from other tau decays and from hadronic events. The 6π mass spectrum is shown in Fig. 22. We measure [27] a branching fraction

$$\mathcal{B}(3\pi^-2\pi^+\pi^0\nu_\tau) = (1.7 \pm 0.2 \pm 0.2) \times 10^{-4}. \quad (65)$$

These results compare well with previous results from CLEO [31,32], ALEPH [33], and OPAL [34], but with smaller errors.

5.3. Resonant substructure in $\tau^- \rightarrow 6\pi\nu_\tau$

Clear signals are seen, and branching fractions measured, for the following decay chains:

- $\tau^- \rightarrow \pi^-2\pi^0\omega\nu_\tau, \omega \rightarrow \pi^+\pi^-\pi^0$

$$\mathcal{B}(\pi^-2\pi^0\omega\nu_\tau) = (1.5 \pm 0.4 \pm 0.3) \times 10^{-4} \quad (66)$$

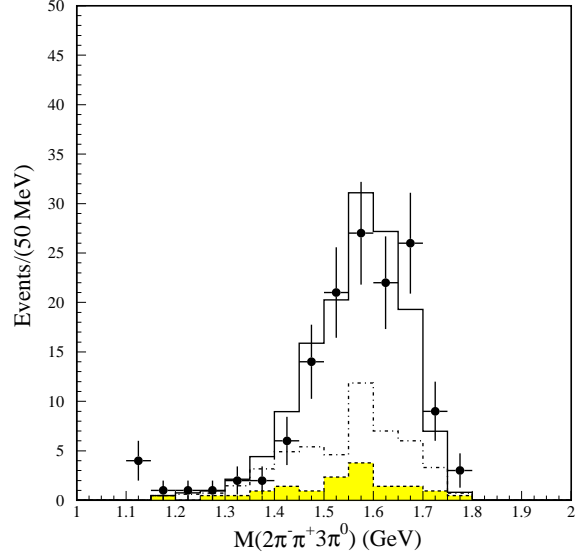


Figure 21. The $m(6\pi)$ spectrum from $\tau^- \rightarrow 2\pi^-\pi^+3\pi^0\nu_\tau$ as measured by CLEO. The points are data. The hatched histogram is an estimate of the hadronic background. The dotted histogram is background from tau decays, and the solid histogram is the prediction for the signal plus backgrounds.

- $\tau^- \rightarrow 2\pi^-\pi^+\eta\nu_\tau, \eta \rightarrow 3\pi^0$

$$\mathcal{B}(2\pi^-\pi^+\eta\nu_\tau) = (2.9 \pm 0.7 \pm 0.5) \times 10^{-4} \quad (67)$$

- $\tau^- \rightarrow \pi^-2\pi^0\eta\nu_\tau, \eta \rightarrow \pi^+\pi^-\pi^0$

$$\mathcal{B}(\pi^-2\pi^0\eta\nu_\tau) = (1.5 \pm 0.6 \pm 0.3) \times 10^{-4} \quad (68)$$

- $\tau^- \rightarrow 2\pi^-\pi^+\omega\nu_\tau, \omega \rightarrow \pi^+\pi^-\pi^0$

$$\mathcal{B}(2\pi^-\pi^+\omega\nu_\tau) = (1.2 \pm 0.2 \pm 0.1) \times 10^{-4} \quad (69)$$

- $\tau^- \rightarrow 2\pi^-\pi^+\eta\nu_\tau, \eta \rightarrow \pi^+\pi^-\pi^0$

$$\mathcal{B}(2\pi^-\pi^+\eta\nu_\tau) = (1.9 \pm 0.4 \pm 0.3) \times 10^{-4}. \quad (70)$$

Some representative sub-mass distributions are shown in Fig. 23. This constitutes the first observation of $\tau^- \rightarrow 2\pi^-\pi^+\omega\nu_\tau$, and the first observations of $\tau^- \rightarrow 3\pi\eta\nu_\tau$ in the $\eta \rightarrow 3\pi$ decay modes.

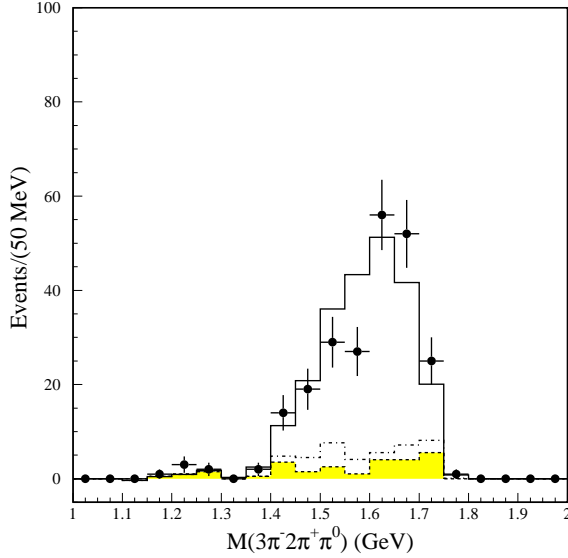


Figure 22. The $m(6\pi)$ spectrum from $\tau^- \rightarrow 3\pi^-2\pi^+\pi^0\nu_\tau$ as measured by CLEO. The points are data. The hatched histogram is an estimate of the hadronic background. The dotted histogram is background from tau decays, and the solid histogram is the prediction for the signal plus backgrounds.

5.4. Separating vector and axial-vector contributions

We can combine these $(3\pi)^-\eta \rightarrow (6\pi)^-$ results with measurements using $\eta \rightarrow \gamma\gamma$ [35], to get:

$$\mathcal{B}_{av}(2\pi^-\pi^+\eta\nu_\tau) = (2.4 \pm 0.5) \times 10^{-4}, \quad (71)$$

$$\mathcal{B}_{av}(\pi^-2\pi^0\eta\nu_\tau) = (1.5 \pm 0.5) \times 10^{-4}. \quad (72)$$

The $(3\pi)^-\eta$ system has a rich substructure, only beginning to be explored; for example, it can arise through the decay chain [35] $f_1\pi$, $f_1 \rightarrow a_0\pi$, $a_0 \rightarrow \eta\pi$.

We can then subtract these contributions from the total $\tau \rightarrow 6\pi\nu_\tau$ decay rate; what's left is presumed to be from the vector current only:

$$\mathcal{B}_V(2\pi^-\pi^+3\pi^0\nu_\tau) = (1.1 \pm 0.4) \times 10^{-4}, \quad (73)$$

$$\mathcal{B}_V(3\pi^-2\pi^+\pi^0\nu_\tau) = (1.1 \pm 0.2) \times 10^{-4}. \quad (74)$$

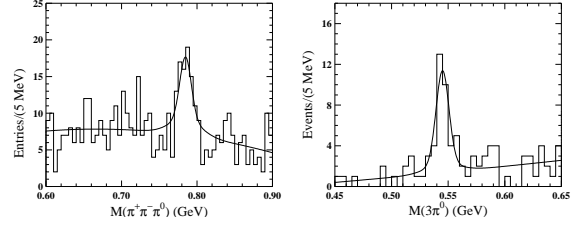


Figure 23. Some sub-mass distributions in $\tau^- \rightarrow 6\pi\nu_\tau$. Left: $m(\pi^+\pi^-\pi^0)$ in $\pi^-2\pi^0\omega\nu_\tau$, $\omega \rightarrow \pi^+\pi^-\pi^0$ (6 entries/event). Right: $m(3\pi^0)$ in $2\pi^-\pi^+\eta\nu_\tau$, $\eta \rightarrow 3\pi^0$ (1 entry/event).

The vector to 6π decay rate \mathcal{B}_V is consistent with being saturated by contributions from $(3\pi)^-\omega$.

From the ratio of these branching fractions, we can constrain the region of the isospin plane, as shown in Fig. 24. Because the rate for $(6\pi)^- \rightarrow \pi^-5\pi^0$ is unknown, we cannot test whether the result lies within the isospin-allowed region.

5.5. CVC predictions for $\tau \rightarrow (6\pi)^-\nu_\tau$

The CLEO results on the vector part of the $\tau \rightarrow 6\pi\nu_\tau$ branching fractions, equations 73 and 74, can be compared with the predictions from $e^+e^- \rightarrow 6\pi$ using CVC [28]:

$$\mathcal{B}_V(2\pi^-\pi^+3\pi^0\nu_\tau) \geq (2.5 \pm 0.4) \times 10^{-4} \quad (75)$$

$$\mathcal{B}_V(3\pi^-2\pi^+\pi^0\nu_\tau) \geq (2.5 \pm 0.4) \times 10^{-4} \quad (76)$$

$$\mathcal{B}_V((6\pi)^-\nu_\tau) \geq (12.3 \pm 1.9) \times 10^{-4} \quad (77)$$

The CVC predictions are significantly higher than the CLEO results. This may be due to an underestimate of the $I = 0$ contributions to $\sigma(e^+e^- \rightarrow 6\pi)$.

6. $\tau^- \rightarrow \nu_\tau\eta(n\pi)^-$

The decay $\tau^- \rightarrow \eta\pi^-\nu_\tau$ is forbidden by G-parity; the upper limit at 95% CL on this decay rate from CLEO [36] is

$$\mathcal{B}(\eta\pi^-\nu_\tau) < 1.4 \times 10^{-4}. \quad (78)$$

The decay $\tau^- \rightarrow \eta\pi^-\pi^0\nu_\tau$ proceeds via the Wess-Zumino chiral anomaly; the branching frac-

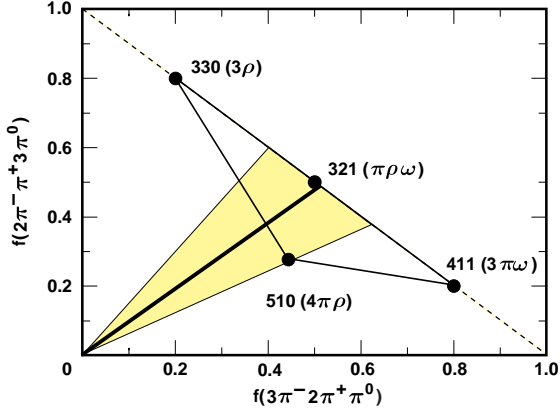


Figure 24. Constraint from CLEO data on the allowed region in the space of 6π partial rate fractions; see Fig. 20.

tion measured by CLEO [36]

$$\mathcal{B}(\eta\pi^-\pi^0\nu_\tau) = (1.7 \pm 0.3) \times 10^{-3}, \quad (79)$$

is in good agreement with predictions. However, the Wess-Zumino Lorentz structure has not been definitively established for this decay.

CLEO sees $\tau^- \rightarrow \eta(3\pi)^-\nu_\tau$ in two modes using $\eta \rightarrow \gamma\gamma$ [35], as well as in the 6π modes reported above. There is rich substructure in these modes, only beginning to be explored. For example, there is evidence of f_1 production [35]: $f_1\pi$, $f_1 \rightarrow a_0\pi$, $a_0 \rightarrow \eta\pi$.

The $SU(3)_f$ -violating decay $\tau^- \rightarrow \eta K^-\nu_\tau$ has been seen by CLEO [37] at the rate

$$\mathcal{B}(\eta K^-\nu_\tau) = (2.6 \pm 0.5) \times 10^{-4}. \quad (80)$$

6.1. $\tau^- \rightarrow K^{*-}\eta\nu_\tau$

The decays $\tau^- \rightarrow K^{*-}\eta\nu_\tau$ were searched for in the CLEO II sample of $\approx 4.3 \times 10^6$ $\tau^+\tau^-$ pairs [38]. In the $\tau^- \rightarrow K_s\pi^-\eta\nu_\tau$ mode, 13 events were observed, with an expected background of 1 event, yielding a product branching fraction:

$$\mathcal{B}(\tau^- \rightarrow K^{*-}\eta\nu_\tau) \times \mathcal{B}(K^{*-} \rightarrow K_s\pi^-) = (1.18 \pm 0.38 \pm 0.12) \times 10^{-4}. \quad (81)$$

In the $\tau^- \rightarrow K^-\pi^0\eta\nu_\tau$ mode, 12 events were observed, with an expected background of 1 event, yielding a product branching fraction:

$$\mathcal{B}(\tau^- \rightarrow K^{*-}\eta\nu_\tau) \times \mathcal{B}(K^{*-} \rightarrow K^-\pi^0) = (0.69 \pm 0.36 \pm 0.28) \times 10^{-4}. \quad (82)$$

Combining the two modes, we obtain

$$\mathcal{B}(K^{*-}\eta\nu_\tau) = (2.90 \pm 0.80 \pm 0.42) \times 10^{-4}, \quad (83)$$

and the mass spectrum shown in Fig. 25. This is the first observation of this decay mode, and it is in reasonable agreement with the prediction of $\sim 1 \times 10^{-4}$ from Ref. [30].

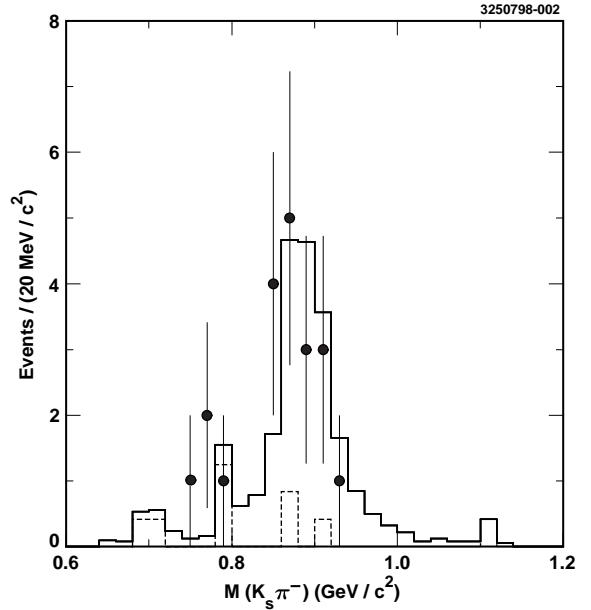


Figure 25. The $M(K_s\pi^\mp)$ spectrum from $\tau^\mp \rightarrow K_s\pi^\mp\eta\nu_\tau$ events observed by CLEO, showing evidence for $K^{*\mp} \rightarrow K_s\pi^\mp$. The points are the data, dashed histogram is the expected background, and solid histogram is the expected signal plus background.

7. Summary and conclusions

We have presented recent results on the structure of the hadronic systems in $\tau \rightarrow 2\pi\nu_\tau, 3\pi\nu_\tau, 4\pi\nu_\tau, 6\pi\nu_\tau$, and modes containing η mesons. There are also new results from CLEO on $\tau \rightarrow Kh\pi(\pi^0)\nu_\tau$ [39] and $\tau \rightarrow K^-\pi^+\pi^-\nu_\tau$ [40], which we have no room to report on here.

There are several apparent ‘discrepancies’ between τ and e^+e^- data. This may be due to normalization problems, other experimental errors, or a real violation of CVC, which is expected at some level. We need a better understanding of the applicability of CVC, to resolve these discrepancies.

The rich structure in multi-meson systems can certainly be further elucidated. It is clear that semi-hadronic tau lepton decay can be a powerful and unique probe of light hadronic systems. The field is still very much driven by experiment. It is hoped that the data will provide stimulation for deeper theoretical work in this difficult field.

The data are also useful for studying other aspects of the Standard Model, such as the tau neutrino helicity h_{ν_τ} , the tau neutrino mass, the running of the strong coupling constant $\alpha_s(m_\tau^2)$, and contributions to vacuum polarization from low energy hadronic physics relevant for predicting the muon anomalous magnetic moment a_μ^{had} and the running EM coupling $\alpha_{em}(M_Z)$.

We can expect more interesting results on low energy meson dynamics in semi-hadronic tau decay, using high-statistics measurements from B factories.

8. Acknowledgements

This submission represents the work of many CLEO collaborators, supported by the US Department of Energy, US National Science Foundation, and other sources. The author would like to thank the organizers for a very stimulating and enjoyable conference in the beautiful city of Victoria.

REFERENCES

1. Y.S. Tsai, Phys. Rev. D4, 2821 (1971).
2. H.B. Thacker and J.J. Sakurai, Phys. Lett. 36B, 103 (1971).
3. CLEO Collaboration, S. Anderson *et al.*, Phys. Rev. D 61, 112002 (2000).
4. Michel Davier, private communication.
5. J.H. Kühn and A. Santamaria, Z. Phys. C 48, 445 (1990).
6. G. Gounaris and J.J. Sakurai, Phys. Rev. Lett. 21, 244 (1968).
7. ALEPH Collaboration, R. Barate *et al.*, Z. Phys. C 76, 15 (1997).
8. Particle Data Group, C. Caso *et al.*, E. Phys. J. C 3, 1 (1998).
9. S. Eidelman and V.N. Ivanchenko, Nucl. Phys. B (Proc.Suppl.) 76, 319 (1999), Proceedings of the Fifth Workshop on Tau Lepton Physics, Santander, Spain, September 1998.
10. R. Alemany, M. Davier and A. Höcker, E. Phys. J. C 2, 123 (1998).
11. J.H. Kühn and F. Wagner, Nucl. Phys. B236, 16 (1984).
12. N. Isgur, C. Morningstar and C. Reader, Phys. Rev. D39, 1357 (1989).
13. N.A. Törnqvist, Z. Phys. C36, 695 (1987); 40, 632(E) (1988). N.A. Törnqvist, Z. Phys. C68, 647 (1995).
14. ARGUS Collaboration, H.Albrecht *et al.*, Z. Phys. C58, 61 (1993); ARGUS Collaboration, H.Albrecht *et al.*, Phys. Lett. 349B, 576 (1995).
15. DELPHI Collaboration, P. Abreu *et al.*, Phys. Lett. 426B, 411 (1998).
16. CLEO Collaboration, D.M. Asner *et al.*, Phys. Rev. D61, 012002 (2000).
17. CLEO Collaboration, T.E. Browder *et al.*, Phys. Rev. D61, 052004 (2000).
18. J.H. Kühn and E. Mirkes, Z.Phys. C56, 661 (1992); erratum Z.Phys. C67, 364 (1995).
19. CLEO Collaboration, M. Athanas, *et al.*, Phys. Rev. D61, 052002 (2000).
20. ARGUS Collaboration, H.Albrecht *et al.*, Phys. Lett. B185, 223 (1987).
21. CLEO Collaboration, P. Baringer, *et al.*, Phys. Rev. Lett. 59, 1993 (1987).
22. ARGUS Collaboration, H.Albrecht *et al.*, Phys. Lett. B260, 259 (1991).
23. ALEPH Collaboration, D. Buskulic *et al.*,

- Z. Phys. C 74, 101 (1997).
24. CLEO Collaboration, K.W. Edwards *et al.*, Phys. Rev. D61, 072003 (2000).
 25. CMD-2 collaboration, Phys. Lett. B475 190 (2000); CMD2 Collaboration, Phys. Lett. B466 392 (1999).
 26. CLEO Collaboration, K.W. Edwards *et al.*, Phys. Rev. D56, 5297 (1997).
 27. CLEO Collaboration, A. Anastassov *et al.*, CLNS 00/1687, CLEO 00-16, submitted to Phys. Rev. D, 2000.
 28. S. Eidelman and V.N. Ivanchenko, Nucl. Phys. B (Proc.Suppl.) 55C, 181 (1997), Proceedings of the Fourth Workshop on Tau Lepton Physics, Estes Park, Colorado, September 1996.
 29. A. Pich, Phys. Lett. B196 (1987).
 30. B.A. Li, Phys. Rev. D55, 1436 (1997); Phys. Rev. D57, 1790 (1998).
 31. CLEO Collaboration, S. Anderson *et al.*, Phys. Rev. Lett. 79, 3814 (1997).
 32. CLEO Collaboration, D. Gibaut *et al.*, Phys. Rev. Lett. 73, 934 (1994).
 33. ALEPH Collaboration, D. Buskulic *et al.*, Z. Phys. C 70, 579 (1996).
 34. OPAL Collaboration, K. Ackerstaff *et al.*, E. Phys. J. C 8, 183 (1999).
 35. CLEO Collaboration, T. Bergfeld *et al.*, Phys. Rev. Lett. 79, 2406 (1997).
 36. CLEO Collaboration, M. Artuso *et al.*, Phys. Rev. Lett. 69, 3278 (1992).
 37. CLEO Collaboration, J. Bartelt *et al.*, Phys. Rev. Lett. 76, 4119 (1996).
 38. CLEO Collaboration, M. Bishai *et al.*, Phys. Rev. Lett. 82, 281 (1999).
 39. CLEO Collaboration, S. Richichi *et al.*, Phys. Rev. D60, 112002 (1999).
 40. CLEO Collaboration, D. Asner *et al.*, CLNS 00/1666, CLEO 00-4, hep-ex/0004002, Submitted to Phys. Rev. Lett. (2000).